**Naval Surface Warfare Center**

**Carderock Division**

West Bethesda, MD 20817-5700

**NSWCCD-80-TR-2022/029** **November 2022**

Naval Architecture and Engineering Department

Technical Report

# APPLICATION OF A POTENTIAL FLOW CODE (PROPCAV) FOR SURFACE PIERCING PROPELLER ANALYSIS

by

Jacob T. Woeste
Thad J. Michael
NSWCCD

# REPORT DOCUMENTATION PAGE

*Form Approved*
*OMB No. 0704-0188*



| **1. REPORT DATE** *(DD-MM-YYYY)* | **2. REPORT TYPE** | **3. DATES COVERED** *(From - To)* |
|---|---|---|
| 23-09-2022 | Final | 04 Oct 2021 – 30 Sept 2022 |

**4. TITLE AND SUBTITLE**
Application of a Potential Flow Code (PROPCAV) for Surface Piercing Propeller Analysis

**5a. CONTRACT NUMBER**

**5b. GRANT NUMBER**

**5c. PROGRAM ELEMENT NUMBER**

**6. AUTHOR(S)**
Woeste, Jacob T.
Michael, Thad J.

**5d. PROJECT NUMBER**

**5e. TASK NUMBER**

**5f. WORK UNIT NUMBER**

**7. PERFORMING ORGANIZATION NAME(S) AND ADDRESS(ES)**
Naval Surface Warfare Center
Carderock Division (Code 872)
9500 Macarthur Boulevard
West Bethesda, MD 20817-5700

**8. PERFORMING ORGANIZATION REPORT NUMBER**
NSWCCD-80-TR-2022/029

**9. SPONSORING / MONITORING AGENCY NAME(S) AND ADDRESS(ES)**
Richard Fonda
Program Manager, 332
Office of Naval Research
Arlington, VA 22217

**10. SPONSOR/MONITOR'S ACRONYM(S)**

**11. SPONSOR/MONITOR'S REPORT NUMBER(S)**

**12. DISTRIBUTION / AVAILABILITY STATEMENT**
DISTRIBURION STATEMENT A. Approved for public release. Distribution is unlimited.

**13. SUPPLEMENTARY NOTES**

**14. ABSTRACT**
A medium-fidelity analysis method for quickly evaluating blade loads for surface piercing propellers with a potential flow unsteady propeller force panel code, PROPCAV, has been evaluated and shown to be viable. Two case studies were examined, consisting of 14.7 in (0.373 m) diameter Mercury Marine Revolution 4 propellers of two different pitches: 21 in (0.533 m) and 23 in (0.584 m) pitches. The results from PROPCAV for maximum and minimum thrust predictions were compared to high-fidelity unsteady Reynolds-averaged Navier-Stokes (U-RANS) computational fluid dynamics (CFD) simulation results and agreed well (within 6.6%).

**15. SUBJECT TERMS**
PROPCAV, Propeller, Surface Piercing, Hydrodynamics, Cavitation, Ventilation

| **16. SECURITY CLASSIFICATION OF:** | | | **17. LIMITATION OF ABSTRACT** | **18. NUMBER OF PAGES** | **19a. NAME OF RESPONSIBLE PERSON** |
|---|---|---|---|---|---|
| **a. REPORT** | **b. ABSTRACT** | **c. THIS PAGE** | | | Jacob T. Woeste |
| Unclassified | Unclassified | Unclassified | Same as Report | 20 | **19b. TELEPHONE NUMBER** *(include area code)* (301)227-2258 |

**Standard Form 298 (Rev. 8-98)**
**Prescribed by ANSI Std. Z39.18**

THIS PAGE INTENTIONALLY LEFT BLANK

## CONTENTS

## FIGURES



## TABLES

## NOMENCLATURE

BEM ..... Boundary-Element Method

CAD ..... Computer-Aided Design

CFD ..... Computational Fluid Dynamics

$C_p$ ..... pressure coefficient, $C_p = \frac{P-P_o}{0.5\rho V_\infty^2}$

$D$ ..... propeller diameter

$Fr$ ..... propeller Froude Number, $Fr = \frac{n^2 D}{g}$

$g$ ..... gravitational acceleration

$h_{\text{tip}}$ ..... maximum propeller tip submergence depth

$J_S$ ..... advance ratio based on ship speed, $J_S = \frac{V_S}{nD}$

$K_Q$ ..... torque coefficient, $K_Q = \frac{Q}{\rho n^2 D^5}$

$K_T$ ..... thrust coefficient, $K_T = \frac{T}{\rho n^2 D^4}$

$n$ ..... propeller revolutions per second

$P$ ..... pressure

$P_o$ ..... pressure far upstream

$P_v$ ..... vapor pressure

PS ..... pressure side

$R$ ..... propeller radius

RPM ..... Revolutions per Minute

SS ..... suction side

$T$ ..... propeller thrust

U-RANS ..... Unsteady Reynolds-Averaged Navier-Stokes

$V_S$ ..... ship speed

$V_\infty$ ..... inflow velocity far upstream

$\rho$ ..... fluid density

$\sigma_n$ ..... cavitation number, $\sigma_n = \frac{P-P_v}{0.5\rho n^2 D^2}$

## ADMINISTRATIVE INFORMATION

This report describes work performed at the Naval Surface Warfare Center, Carderock Division (NSWCCD) in West Bethesda, MD by the Propulsors Branch (Code 872) in the Naval Architecture and Engineering Department (Code 80). The work was sponsored by the Office of Naval Research (ONR) as part of the 'Agile Manufacturing Integrated Computational Materials Engineering (ICME) Toolkit' project.

## ACKNOWLEDGEMENTS

The authors thank Seungnam Kim (University of Texas at Austin) for his help debugging PROPCAV for surface piercing applications.

## SUMMARY

A medium-fidelity analysis method for quickly evaluating blade loads for surface piercing propellers with a potential flow unsteady propeller force panel code, PROPCAV, has been evaluated and shown to be viable. Two case studies were examined, consisting of 14.7 in (0.373 m) diameter Mercury Marine Revolution 4 propellers of two different pitches: 21 in (0.533 m) and 23 in (0.584 m) pitches. The results from PROPCAV for maximum and minimum thrust predictions were compared to high-fidelity unsteady Reynolds-averaged Navier-Stokes (U-RANS) computational fluid dynamics (CFD) simulation results and agreed well (within 6.6%).

## INTRODUCTION

The Agile nickel-aluminum bronze (NAB) thrust project within the 'Agile Manufacturing Integrated Computational Materials Engineering (ICME) Toolkit' program seeks to leverage ICME techniques for large-scale additive manufacturing of propellers, particularly those made of NAB. The technical goal of this part of the project was to assess the additive manufacturing built structure by mapping surface pressures from CFD analysis to finite element grids for structural analysis. The overarching goal was to develop collaboration methods and Carderock's tools for carrying out such a task in a timely manner. The focus was on the process, and no tangible propeller design was to be delivered. The work presented in this paper is intended to document the propeller hydrodynamic analysis efforts to obtain the blade pressure loads needed for later structural analysis by Carderock's Submarine Structures & Propulsors Branch (Code 652).

Two case studies were examined, consisting of 14.7 in (0.373 m) diameter Mercury Marine Revolution 4 surface piercing propellers with 21 in (0.533 m) and 23 in (0.584 m) pitches, which are termed the 21p and 23p propellers, respectively. Both propellers have the same general characteristics besides their different pitches, as summarized in Table 1.

**Table 1. Mercury Revolution 4 21p and 23p Propeller Characteristics**

| | |
|---|---|
| Propeller Diameter ($D$) | 14.7 in (0.373 m) |
| Hub to Tip Diameter Ratio | 0.35 |
| Number of Blades | 4 |
| Shaft Inclination Angle | 10° |
| Max Propeller Tip Submergence Ratio ($h_{\mathrm{tip}}/D$) | 0.6 |

The Propeller Cavitation Computer Code (PROPCAV) is a boundary-element method (BEM) potential flow panel code developed by the University of Texas at Austin. PROPCAV is capable of hydrodynamic analyses of surface piercing propellers with sheet cavitation and ventilation [1]. As a BEM potential flow panel code, PROPCAV can capture the major physics involved and predict blade surface pressures orders of magnitude faster than high-fidelity U-

RANS CFD simulations. PROPCAV is widely applied for submerged propeller analyses and has not been applied extensively for surface piercing blade loading analysis applications, so its effectiveness for quickly predicting blade loads is discussed in this work by comparing PROPCAV's predictions with those from U-RANS CFD. The U-RANS CFD results were provided by Carderock's Computational Fluid Dynamics Branch (Code 871) from STAR-CCM+ [2]. The version of PROPCAV was a beta version, containing changes not yet fully tested or officially released by the University of Texas at Austin.

## METHODOLOGY

### Geometry Creation

The propeller geometries for the 21p and 23p were provided as computer-aided design (CAD) files. The CAD geometry was sliced at constant radii to produce a set of blade section surface points in 3D space by Rhino [3]. These section points were then fed into propeller geometry extraction codes to obtain the geometry input format for PROPCAV.

Some minor approximations of the original geometry were needed for PROPCAV to successfully run in surface piercing analysis mode. First, a closed geometry was needed, so the camber and thickness of the blade at the tip were changed to be zero. Second, an open trailing edge was needed, and the trailing edge had to be cut at a constant chord location. Therefore, either the suction side (SS) or pressure side (PS) of the trailing edge needed to be trimmed. The suction side of a surface piercing propeller has sheet cavitation and ventilation, so its trailing edge geometry is engulfed in the sheet, rendering its geometry less important than the pressure side to obtain the correct thrust and loading of the blade. Therefore, the suction side trailing edge geometry was trimmed in Figure 1 at 40% radius ($R$). In the figure, $x$ is the chord-wise coordinate along the nose-tail line and $y$ is the direction perpendicular to the nose-tail line in the cylindrical cutting plane.

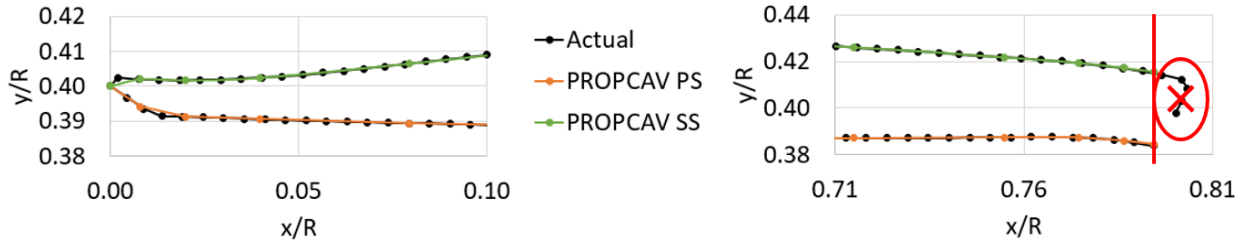


**Figure 1. Leading Edge (Left) and Trailing Edge (Right) Geometry Comparisons between the Actual CAD Geometry and the Representation of the Geometry in PROPCAV at 40% Radius**

In Figure 1, the leading edge geometry was captured well in PROPCAV. The trailing edge geometry was also captured well hydrodynamically, when the suction side trailing edge was trimmed (emphasized by the red markings in Figure 1) because the suction side trailing edge was expected to be in a cavity. The final representation of the 21p propeller geometry in PROPCAV is compared to the CAD geometry in Figure 2, where 30 chord-wise and 15 span-wise blade panels approximated the geometry. This resolution was the finest grid that allowed for the PROPCAV solution to converge and produce results. The 23p propeller was nearly the same.

CAD PROPCAV

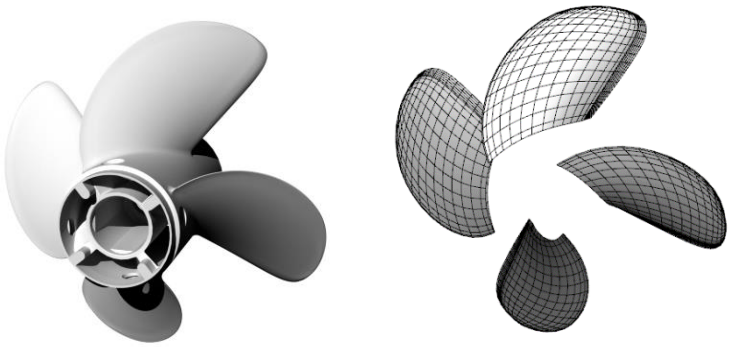

**Figure 2. 21p Propeller Geometry Comparison.**

The hub geometry was excluded for the runs in PROPCAV discussed in this paper because solutions without the hub panels produced the closest results for total thrust compared to STAR-CCM+'s U-RANS CFD simulations, which included the outboard lower unit geometry ahead of the propeller and the hub geometry. For perspective, using a cylindrical panel hub in PROPCAV further under-predicted total thrust by 7%.

## Operating Points

Mercury Marine provided the operating conditions for the 21p propeller, which are summarized in Table 2. The advance coefficient ($J_S$), propeller Froude Number ($Fr$), and cavitation number ($\sigma_n$) are defined in the Nomenclature section. This operating condition was used for the simulations in PROPCAV and STAR-CCM+'s U-RANS CFD solver. The operating point for the 23p propeller, also in Table 2, was derived to match the 21p propeller blade section angle of attack at 70% radius for the same vessel speed. Since the 23p propeller had a larger pitch angle, it had to operate at a lower revolutions per minute (RPM) to match the blade section angle of attack of the 21p propeller. A uniform inflow was applied in PROPCAV for the analysis, and the operating points in Table 2 were used, with the exception that $\sigma_n$ had to be 0 due to the surface piercing operating condition.

**Table 2. 21p and 23p Propeller Operating Points**

| | 21p | 23p |
|---|---|---|
| $V_S$ | 56 kts (29 m/s) | 56 kts (29 m/s) |
| RPM | 3492 | 3143 |
| $J_S$ | 1.3 | 1.5 |
| $Fr$ | 129 | 104 |
| $\sigma_n$ | 0.43 | 0.53 |

# RESULTS

## 21p Total Thrust

The 21p propeller was simulated at the operating conditions described previously. The total thrust generated for one propeller revolution is compared between PROPCAV and STAR-CCM+'s U-RANS CFD solver in Figure 3, where 0 degrees corresponds with when the mid-chord of the root blade section is at the uppermost position during the propeller rotation. Four peaks exist in total thrust due to the propeller having four blades. From the results in Figure 3, a phase shift exists where the peak thrust occurred, and this peak was slightly less for the U-RANS prediction than the PROPCAV prediction. This is likely due to free surface elevation differences caused by the omission of the outboard lower unit geometry ahead of the propeller in PROPCAV, which was included in the STAR-CCM+ U-RANS solver. Since the U-RANS simulation included the strut and lower unit geometry ahead of the propeller and included viscous flow interaction effects, the free surface was drawn upwards along the strut, causing the propeller to be more submerged than in PROPCAV because PROPCAV can only account for the calm water free surface. The minimum thrust occurred near the same angular position but was of a lower magnitude according to PROPCAV due to similar reasons. A comparison of the maximum and minimum thrust magnitudes is included in Table 3 and Table 4, where the thrust coefficient ($K_T$) and torque coefficient ($K_Q$) are defined in the Nomenclature section.

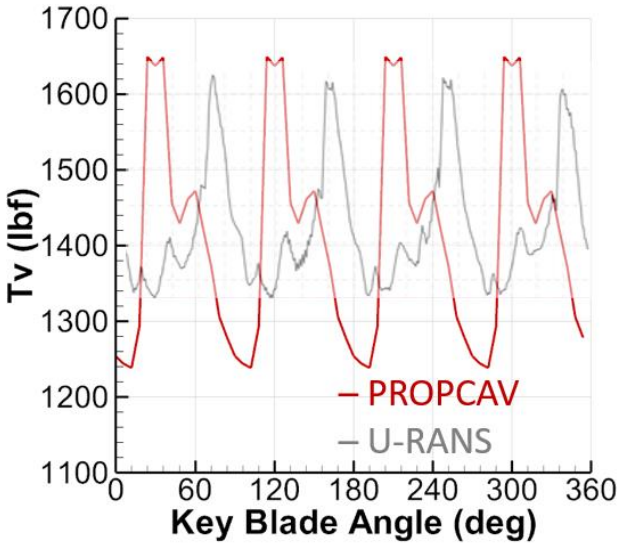


**Figure 3. 21p Total Thrust Comparison between PROPCAV and U-RANS for One Propeller Revolution**

**Table 3. 21p Maximum Thrust Comparison between PROPCAV and U-RANS**

| | PROPCAV | U-RANS | % Difference from U-RANS |
|---|---|---|---|
| Max Thrust | 1649 lbf (7335 N) | 1625 lbf (7228 N) | 1.5% |
| Max $K_T$ | 0.113 | 0.111 | |

**Table 4. 21p Minimum Thrust Comparison between PROPCAV and U-RANS**

| | PROPCAV | U-RANS | % Difference from U-RANS |
|---|---|---|---|
| Min Thrust | 1238 lbf (5507 N) | 1325 lbf (5894 N) | -6.6% |
| Min $K_T$ | 0.085 | 0.091 | |

From the results in Table 3, PROPCAV over-predicted maximum total thrust by 1.5% relative to the U-RANS results. Likewise in Table 4, PROPCAV predicted a lower minimum total thrust than U-RANS by 6.6%. The root cause of these slight differences will be discussed in the following section from the blade pressure distributions.

## 21p Blade Pressure Distributions

Blade pressure distributions are important for determining structural loads of each blade. The blade pressure on the suction side of the blades was essentially the same between the PROPCAV and U-RANS predictions because the suction side was almost completely covered with cavities due to ventilation and cavitation, in Figure 4. In the purple regions that represent cavities in Figure 4, the blade surface pressure coefficient ($C_p$, defined in the Nomenclature section) is zero. Since blade suction side pressures were similar, to compare blade pressure side pressures was more useful, which had larger portions that were wetted. A comparison of the pressure side pressure distribution predictions by PROPCAV and U-RANS is shown at their respective maximum total thrust condition in Figure 5.

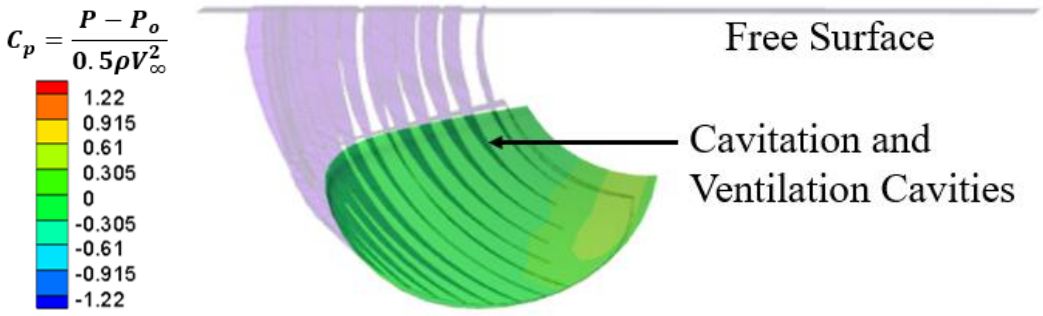


**Figure 4. Submerged 21p Blade Showing Suction Side Blade Pressure Distribution and Cavity Profiles Predicted by PROPCAV**

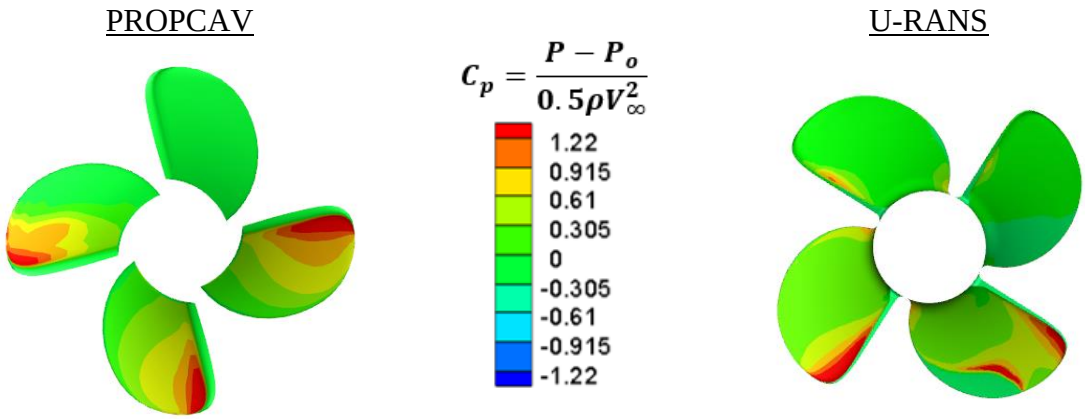


**Figure 5. 21p Pressure Side Blade Pressure Distributions from PROPCAV (Left) and U-RANS (Right) at the Maximum Total Thrust Condition**

The U-RANS blade pressure distributions in Figure 5 suggest that multiple cavities were present on the lower right blade at the maximum thrust condition, as represented by the separate red contour regions from mid-span to the tip. PROPCAV predicted a different rotational position for the total maximum thrust condition, and the pressure contours on all of its blades revealed that only one cavity per radial position existed. The major differences between PROPCAV and U-RANS at the maximum thrust condition were due to PROPCAV's inability to predict multiple cavities per side per radius. Once a blade pierces the water surface in PROPCAV and begins cavitating and ventilating, the blades no longer have intermittent wetted areas between cavities at a certain radius. This caused the peak thrust to occur at a different rotational position in PROPCAV, where the majority of three blades were submerged. According to U-RANS, the peak thrust occurred when the majority of two blades were submerged because that was when the cavities broke apart for one of the blades, which allowed for more wetted surface area on the pressure side to generate more thrust. A similar comparison is presented in Figure 6 for the minimum thrust condition.

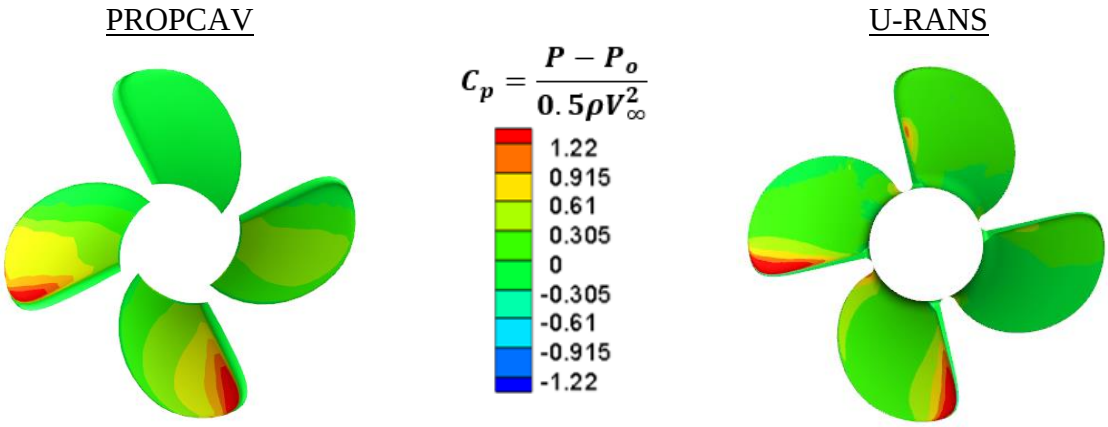


**Figure 6. 21p Pressure Side Blade Pressure Distributions from PROPCAV (Left) and U-RANS (Right) at the Minimum Total Thrust Condition**

The pressure distributions were similar for the minimum total thrust condition in Figure 6. Only one cavity per radius was predicted by both simulations at this condition, and the rotational position of the minimum thrust condition was similar as a consequence. A comparison of the thrust generated by each individual blade for both simulations at the exact same rotational position, which corresponds with the U-RANS maximum thrust condition, is in Table 5, where the blade numbering scheme is at the bottom of the table.

**Table 5. 21p Individual Blade Thrust Comparisons at the Same Propeller Rotational Position**

| Blade | PROPCAV Thrust | U-RANS Thrust | Difference Relative to U-RANS Total |
|---|---|---|---|
| 1 | -38.9 lbf (-173 N) | -51.6 lbf (-230 N) | 0.8% |
| 2 | 0.0 lbf (0.0 N) | 120 lbf (534 N) | -7.5% |
| 3 | 709 lbf (3,154 N) | 843 lbf (3,750 N) | -8.3% |
| 4 | 701 lbf (3,118 N) | 703 lbf (3,127 N) | -0.1% |
| Total | 1,372 lbf (6,103 N) | 1,616 lbf (7,188 N) | -15.1% |


In Table 5, the largest errors in individual blade thrust predictions between the PROPCAV and U-RANS simulations were for blades 1, 2, and 3. Blades 1, 2, and 3 were each partially emerged from the calm water free surface, and their larger differences were an indication that certain interactions present in the U-RANS simulation were not captured in the PROPCAV simulation. PROPCAV predicted blade 2 to be fully emerged from the water (no generated thrust), whereas U-RANS predicted the blade to be partially submerged with 120 lbf (534 N) generated thrust. Since the U-RANS simulation included the strut and lower unit geometry ahead of the propeller and included viscous flow interaction effects, the free surface was drawn upwards along the strut, causing the propeller to be more submerged than that in PROPCAV because PROPCAV can only account for the calm water free surface. Therefore, this effect can be compensated somewhat in PROPCAV by artificially adjusting the propeller submergence.

In Table 5, the thrust generated by blade 4 was predicted to be nearly the same between the two simulations (within 0.1%) even though the blade 4 pressure distributions were very different. U-RANS predicted multiple cavities per radius whereas PROPCAV was only able to predict one (multiple red pressure contour areas in U-RANS vs. only one in PROPCAV). Even though the total thrust for blade 4 was the same between the two simulations, the blade loading was different due to PROPCAV's inability to predict multiple cavities per radius, which will lead to different blade stresses.

### 23p Blade Pressure Distributions

The 23p propeller was also simulated in PROPCAV to demonstrate the capability to simulate another propeller geometry. A comparison of the 23p and 21p propeller pressure coefficient distributions is in Figure 7 at their maximum total thrust condition and Figure 8 at their minimum total thrust condition. The pressure coefficient contours and magnitudes were similar, which was expected due to both propellers operating at approximately the same blade angle of attack. The rotational positions for maximum and minimum total thrust conditions were also the same. This demonstrated that the process for quickly determining blade pressure loads of surface piercing propellers in PROPCAV can be applied to other similar propeller geometries.

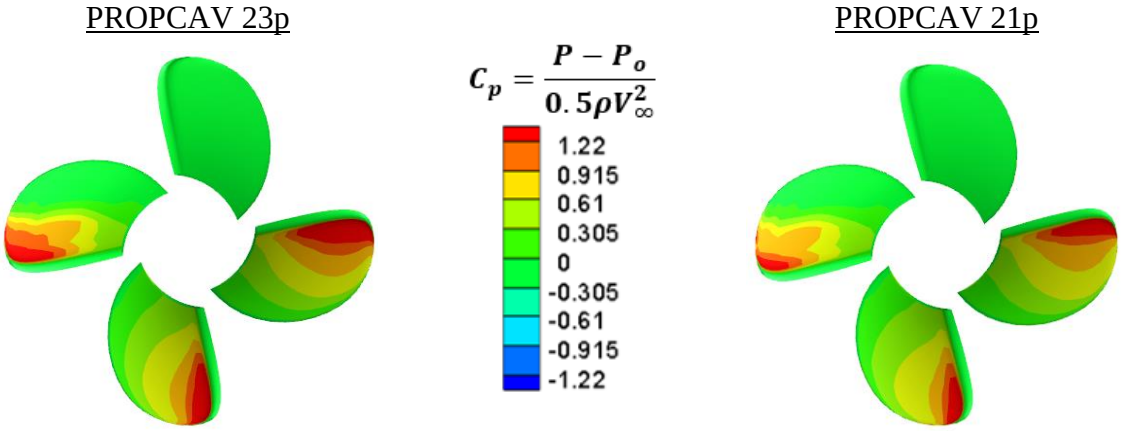


**Figure 7. PROPCAV Pressure Side Blade Pressure Distributions from the 23p (Left) and 21p (Right) Propellers at their Maximum Total Thrust Conditions**

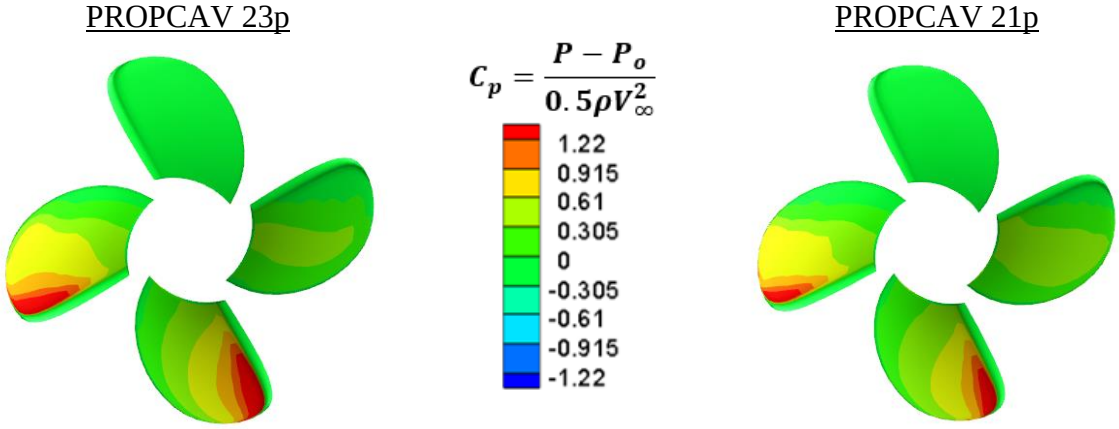


**Figure 8. PROPCAV Pressure Side Blade Pressure Distributions from the 23p (Left) and 21p (Right) Propellers at their Minimum Thrust Conditions**

## CONCLUSIONS

PROPCAV was determined to be an effective solver for surface piercing propellers with sheet cavities. PROPCAV's predictions of maximum and minimum total thrust for the 21p propeller were within 6.6% of STAR-CCM+'s U-RANS results. The differences between PROPCAV and U-RANS for propeller thrust and blade pressure distributions were primarily due to PROPCAV's inability to accurately account for free surface elevation changes caused by the lower unit geometry ahead of the propeller and inability to account for multiple blade cavities per side per radius. Artificially adjusting the propeller submergence in PROPCAV could somewhat compensate for the errors due to blade submergence effects. The 23p propeller was also analyzed in PROPCAV and found to have similar predictions. The process for quickly determining blade pressure loads of surface piercing propellers in PROPCAV can be applied to other similar propeller geometries.

## REFERENCES

[1] Kim, S., Du, A., and Kinnas, S. A., "PROPCAV User Manual and Documentation." The University of Texas at Austin Report No. 19-1, Sept. 2019.
[2] "STAR-CCM+ User Manual." Siemens, 2021.
[3] "Rhino User's Guide for Windows." Robert McNeel & Associates, 24 Nov. 2021.

THIS PAGE INTENTIONALLY LEFT BLANK

## Distribution

| | *Digital Copies* |
|---|---|
| Defense Technical Information Center<br>8725 John J. Kingman Road<br>Ft. Belvoir, VA 22060-6218 | 1 |
| Chief of Naval Research<br>Attn: Code 332<br>Office of Naval Research<br>875 North Randolph Street<br>Arlington, VA 22217<br>Attn: Fonda, Mullins, Wolk | 3 |
| Commander<br>Attn: Code 6356, 6394<br>US Naval Research Laboratory<br>4555 Overlook Ave SW<br>Washington, DC 20375<br>Attn: Birnbaum, Iliopoulos, Michopoulos, Rowenhorst, Steuben | 5 |
| Mercury Marine<br>W6250 Pioneer Road<br>Fond du Lac, WI 54936-1939<br>Attn: John Scherer | 1 |

**NSWC, CARDEROCK DIVISION INTERNAL DISTRIBUTION**

| Code | Name | *Hard Copies* | *Digital Copies* |
|---|---|---|---|
| 604 | C. Waters | | 1 |
| 611 | C. Fisher | | 1 |
| 809 | D. Intolubbe | | 1 |
| 872 | J. Woeste | | 1 |
| 1033 | TIC - SCRIBE | | 1 |


NAVSEA
WARFARE CENTERS
Carderock